Journal of Power Sources 239 (2013) 9–15

Contents lists available at SciVerse ScienceDirect

Journal of Power Sources

journal homepage: www.elsevier.com/locate/jpowsour

Short communication

Fast charging technique for high power lithium iron phosphate batteries: A cycle life analysis

D. Anseán [a,*], M. González [a], J.C. Viera [a], V.M. García [b], C. Blanco [a], M. Valledor [a]

[a] University of Oviedo, Department of Electrical Engineering, Campus de Gijón, Módulo 3, 33204 Gijón, Asturias, Spain
[b] University of Oviedo, Department of Physical and Analytical Chemistry, Campus de Gijón, Edificio Polivalente, 33204 Gijón, Asturias, Spain

HIGHLIGHTS

- A multistage fast charging technique on lithium iron phosphate cells is proposed.
- An extended cycle life study (4500 cycles) is performed.
- The proposed charging algorithm permits fully recharging the cell in approximately 20 min and is energy efficient.
- Special attention has been paid to the impact of fast charging on long-term effects.

ARTICLE INFO

Article history:
Received 26 July 2012
Received in revised form
14 December 2012
Accepted 12 March 2013
Available online 26 March 2013

Keywords:
Fast charging
Cycle life
Lithium iron phosphate battery
Electric vehicle

ABSTRACT

Reduction of the charging time for batteries is a crucial factor in the promotion of consumer interest in the commercialization of electric vehicles (EVs). Fast charging methods for EVs are therefore important to create and understand; however, fast charging is not tolerated by all lithium-ion chemistries because it typically affects the battery functionality and accelerates its aging mechanisms. A fast charging technique is proposed in this paper, and the results of extensive testing on a high power lithium iron phosphate cell subjected to the method are reported. The evaluation characterized the cell's capacity fade, cycle life, and energy efficiency with respect to the U.S. Advanced Battery Consortium (USABC) goals. The proposed charging algorithm permits a full recharging of the cell (0–100% SOC) in approximately 20 min, even after 4500 cycles are reached. The cycling scheme is characterized by high current discharges that reach specific powers of 400 W kg^{-1}. The results show that the proposed fast charging technique does not introduce any significant degradation effects on the cell and is energy efficient; they also show that performance is lost due to capacity fade rather than an increase in internal resistance.

1. Introduction

Nowadays, to fully recharge EVs using a Level II-240 V charging station takes from six to 8 h [1,2]. This charging time is moderately long and becomes impractical when on-site recharges are needed (e.g., when traveling long distances). To overcome this issue, Level III fast-charging power levels have been defined and implemented, although they vary from country to country [3]. More importantly, this fast charging feature is not available on all EVs [4] because the high current causes degradation of the batteries and reduces their lifetime. Few EV manufacturers allow fast charging, and it is recommended that it be used infrequently to minimize battery degradation.

According to the U.S. Advanced Battery Consortium (USABC), the long term goal for fast charging is to return 40% of the state of charge (SOC) of the battery within 15 min [5]; however, fast charging typically involves high current rates, high energy throughputs and high temperatures, all of which force the deterioration of a battery's electric characteristics [6] and affect its functionality. Only advanced chemistries that are capable of fast charging can tolerate these stressful conditions without significant deterioration. As a consequence, few battery manufacturers can presently provide cells that both accept fast charging and have a long lifetime.

In recent years, major advances in lithium-ion (Li-ion) batteries have led to their use as a viable technology for energy storage systems, power electric applications and, most recently, the electric vehicle (EV) automotive industry. A wide variety of lithium-based chemistries are presently used in the electric automotive world as cathode materials, including lithium iron phosphate (LFP), lithium

* Corresponding author. Tel.: +34 985 182 559; fax: +34 985 182 138.
E-mail address: anseandavid.uo@uniovi.es (D. Anseán).

0378-7753/$ – see front matter © 2013 Elsevier B.V. All rights reserved.
http://dx.doi.org/10.1016/j.jpowsour.2013.03.044

nickel cobalt aluminum oxide (NCA) and lithium nickel cobalt manganese oxide (NMC) [7,8]. Among the multiple Li-ion choices, LFP is projected to capture a significant part of the EV industry because of its key advantages: intrinsic safety, low cost, high cycle-lifetime, high power capability, reliability, widespread availability of materials, low toxicity and flat voltage profile. In contrast, the main disadvantages of the LFP technology are its lower voltage, poor lithium diffusion and poor electronic conductivity [9,10]. Despite these disadvantages, much progress has been made to improve the overall performance of the LFP technology [11,12].

Specific fast charging techniques based on various chemistries have been previously reported. Examples include boost charging with lithium cobalt oxide (LCO) [13] and constant current fast charging with lithium titanate oxide (LTO) [14]. The charging protocol also plays an important role in the cycle life of the cell for LCO chemistry [15]. However, a fast charging proposal with an extensive cycling analysis for over 4500 cycles on LFP chemistry has not been reported.

A multistage fast charging technique for high power LFP cells is proposed in this paper. Extended cycle-life testing (up to 4500 cycles) was performed to detect long-term degradation effects on the cell. The tested cell was accurately analyzed for its capacity fade, efficiency, temperature, and internal resistance evolution with cycling. USABC goals such as specific power (W kg^{-1}), energy efficiency and cycle life were also studied in the proposed cycling scheme.

This study provides useful information for the potential use of fast charging in EVs, PHEVs, and Battery Management System (BMS) designs. Furthermore, the data obtained from the tests carried out in this work could be used in follow up studies on cell degradation mechanisms [16].

2. Experimental

2.1. Battery test procedures

Nanophosphate® high power LFP cells manufactured by A123Systems were used in this work. Material enhancement in these cells considerably improves their conductivity and rate capability in comparison to standard LFP cells [12]. According to the manufacturer, these cells allow fast charging and high discharging rates, and they are suitable for portable high power devices, commercial trucks and bus hybrid electric vehicles (HEVs) [17]. The manufacturer's product datasheet shows that these cells weigh an average of 70 g and have a capacity of 2.3 Ah.

The LFP cell was subjected to the battery testing procedures shown in Fig. 1. The test started with commissioning, in which the battery was identified and weighed, and the open circuit voltage (OCV) was measured. Next, the conditioning test sequence was performed according to the USABC constant current discharge series [5]. The cell was charged according to the standard charging method provided by the manufacturer, which consists of a constant current stage at 1 C until the cell reaches 3.6 V, followed by a constant voltage stage until the current declines to C/20. Subsequent to the capacity stabilization, a final charge/discharge cycle was performed at a rate of C/25. Measurements at this slow rate provide a practical capacity reference with minimal kinetic effects that is close to the maximum capacity attainable by the cell [16,18].

The cycling procedure started after the conditioning of the cell was finished. This cycling scheme consisted of a series of continuous full charge and discharge cycles. The charging was performed using the proposed fast charging technique, whereas the discharge was carried out at 4 C constant current until the 2 V cut-off voltage was reached. This sequence was performed continuously for 300 cycles, after which the reference tests were performed.

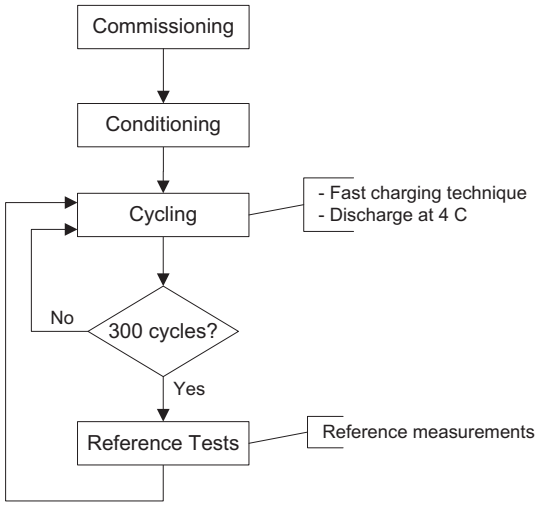

Fig. 1. Flow diagram of the testing procedure.

The test sequence included two cycles with standard charges at 1 C and discharges at 1 C and C/3, followed by a final constant current charge and discharge cycle at C/25. This set of reference tests was used to characterize the degradation that occurs during the life of the subject test unit and to measure the cell's maximum achievable capacity and internal resistance. The resistance of the cell versus the SOC can be calculated from Ohm's law (Eq. (1)) using the cell voltage difference when two different currents are applied [19]:

$$R_{I1-I2(\mathrm{SOC})} = \frac{U_{I1(\mathrm{SOC})} - U_{I2(\mathrm{SOC})}}{I1 - I2} \quad (1)$$

The cycling procedure was started again after each of the reference tests was finished.

The tests were carried out using a multichannel Arbin BT-2000 battery testing system. A Memmert environmental chamber was used to maintain a constant ambient temperature of 23 °C. The temperatures in both the climate chamber and the cell case were measured with T-type copper-constantan thermocouples and logged into the Arbin system.

2.2. Fast-charging protocol

The proposed multistage fast charging technique profile is shown in Fig. 2. The charging process is split into three different stages, referred as CC-I, CC-II and CV-I. The first stage (CC-I) starts with a constant current at 4 C to the charging cut-off voltage (3.6 V). The second stage (CC-II) is a constant current charge at 1 C. Since the current in CC-II is lower than in CC-I, the cell voltage drops below 3.6 V (see Fig. 2 (b)) allowing the charge to be extended, until the cell reaches again the charging cut-off voltage. The last stage (CV-I) is performed at a constant voltage of 3.6 V for a duration of 5 min. The SOC is shown in Fig. 2 (c); it increases linearly as the cell is charged at constant current and asymptotically during the constant voltage stage. Fig. 2 (d) shows the cell temperature evolution. The temperature is reminiscent of a symmetric bell curve over time: it starts at an ambient temperature of 23 °C, increases by 2 °C to its maximum at approximately half the charging time, and ends back at the ambient temperature.

The multistage fast charging technique is based on the evolution of internal resistance during the charging sequence. Fig. 3 shows the results of the internal resistance evolution versus the SOC for charging calculated with Eq. (1) using C/25 and 4 C currents. The internal resistance reaches its minimum immediately after starting

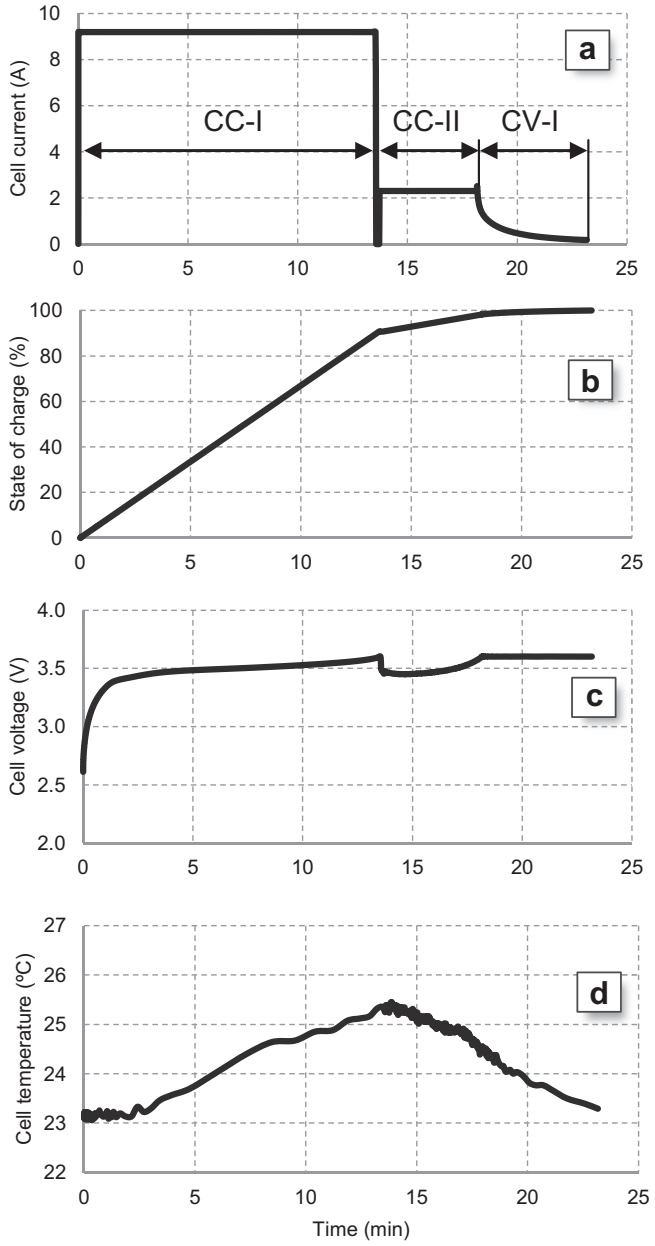

Fig. 2. Current, voltage, state of charge and temperature profiles for the fast-charging technique.

the charging process. As the cell reaches approximately 10% SOC, the internal resistance remains practically constant at 15–16 mΩ until 70% SOC is achieved, after which the internal resistance value increases rapidly. This internal resistance behavior has been reported for LFP prototype power cells from the same manufacturer [19].

Because of the internal resistance behavior, the highest charging current 4 C is applied when the cell's internal resistance is at the lower values. This approach results in a more energy efficient charging process. The last two stages of the charging process are applied as the cell's internal resistance increases rapidly; this procedure helps to decrease the cell's temperature to its initial value (see Fig. 2 (d)). The charging current rate at 4 C was selected because it is close to the maximum charging current recommended by the manufacturer (10 A); a security margin of 12% was selected to avoid working at the limiting current, which reduced the

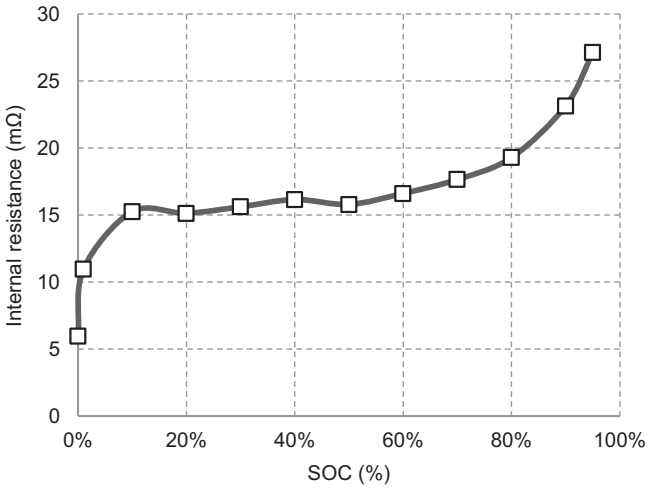

Fig. 3. Internal resistance evolution profile versus state of charge of the cell.

likelihood of overheating. The last stage of the fast-charging procedure provides better cell preservation by limiting constant voltage charging to 5 min, thus avoiding an acceleration of the aging process that occurs at high SOC values over longer periods of time [12].

3. Results

3.1. Conditioning results

Prior to cycling, conditioning tests were carried out to determine the effective capacity of the testing cell under specific current rates. The nominal capacity adopted for this work was obtained from the conditioning tests carried out at 1 C: 2.267 ± 0.001 Ah during the charge and 2.264 ± 0.001 Ah during the discharge. The average capacities measured in the characterization tests are shown in the bar chart of Fig. 4. The highest capacity delivered by the cell was measured during the C/25 test and achieved a value 2.5% greater than that of the 1 C test. The coulombic efficiency was calculated for all of the tests and was invariably near 100%.

Fig. 5 depicts three different cell discharge curves ranging from C/25 to 1 C. The discharge curve shapes are similar to each other and have a conveniently flat voltage profile.

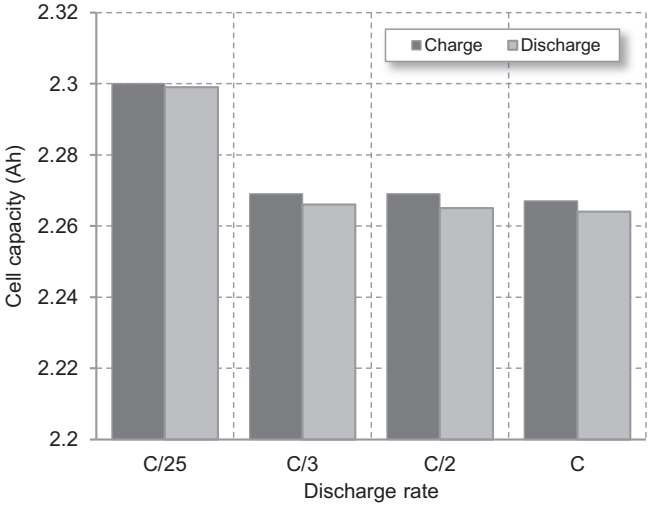

Fig. 4. Cell capacity under different regimes.

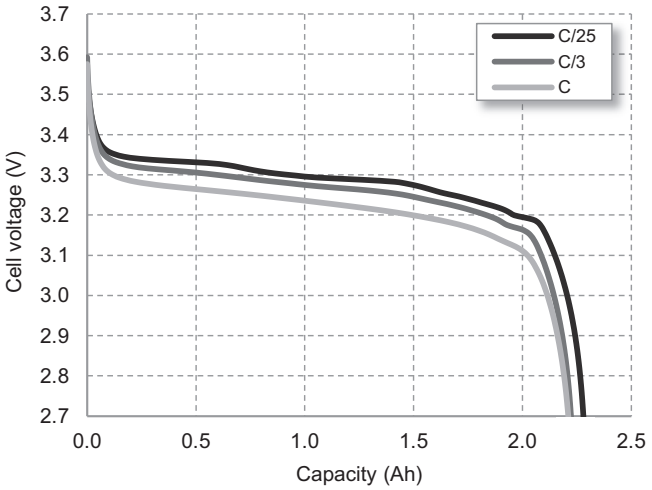

Fig. 5. Voltage discharge curves at C/25, C/3 and C.

The average energy delivered by the cell under the conditioning tests is presented in the bar chart shown in Fig. 6. The energy efficiency was calculated as the ratio of the net DC energy delivered by the cell to the total DC energy required to restore the initial SOC. For the energies shown in Fig. 6, the efficiency values are 98.95% at C/25, 96.10% at C/3, 95.66% at C/2 and 94.89% at 1 C.

Based on the measurements of weight (73.42 g) and energy, the cells exhibited a specific energy of 102.4 Wh kg^{-1}, 100.1 Wh kg^{-1}, 99.72 Wh kg^{-1} and 98.82 Wh kg^{-1} for discharge rates of C/25, C/3, C/2, and 1 C, respectively.

3.2. Cycling scheme: fast charge protocol results

The evolution of the charged capacity and charging time during the different charging stages and cycles is shown in Fig. 7(a–b). As it can be seen, almost all of the cell's capacity is charged during the first stage at 4 C. Ninety percent of the cell charged capacity is filled in less than 15 min (≈60% of the total charging time), even after 4500 cycles. The second stage at 1 C uses 4–5 min (≈20% of the total charging time) to charge the 6–7% of the cell capacity. The final stage is the least efficient with respect to time and charge capacity because it only charges approximately 1.5% of the total charged capacity in 5 min (≈20% of the total charging time). The

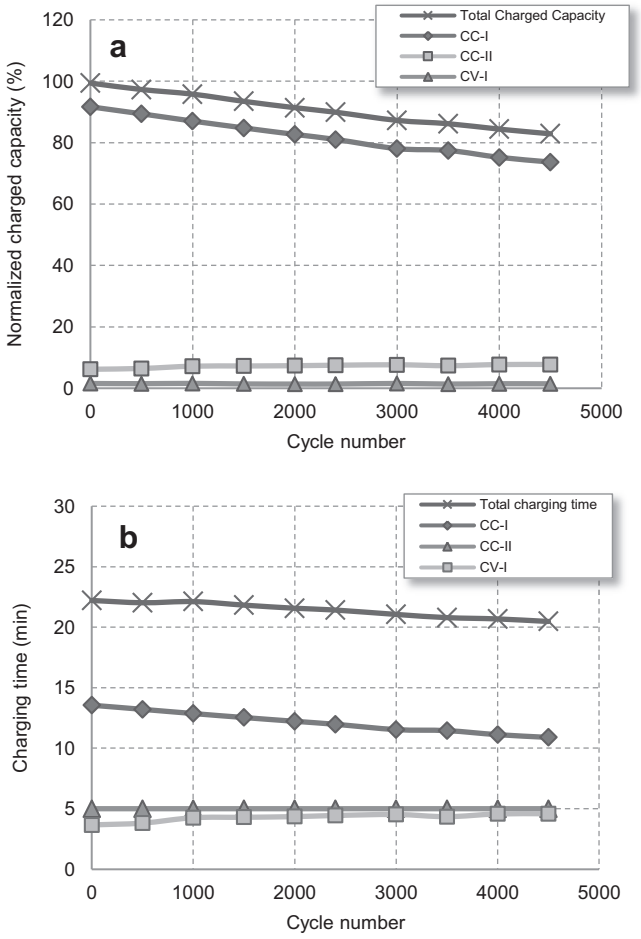

Fig. 7. (a) Charged capacity versus cycle number using the proposed fast charging technique. (b) Charging time versus cycle number using the proposed fast charging technique.

two last stages charge the last 10% of the cell charged capacity taking 40% of the total charging time, but they allow the cell temperature to decrease.

Fig. 8 reveals that recharging can be performed very quickly with the proposed fast charging technique. The cell is charged from 0% to 40% of its capacity in approximately 6 min; these values meet the USABC goals regarding fast charging. In addition, the cell is fully

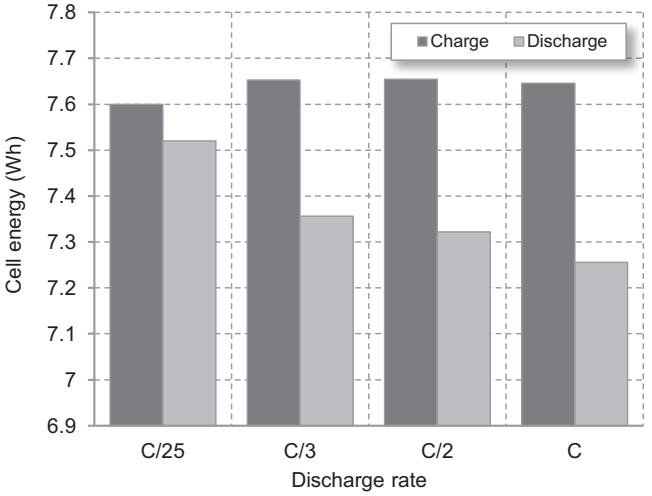

Fig. 6. Charge and discharge average energies for different rates.

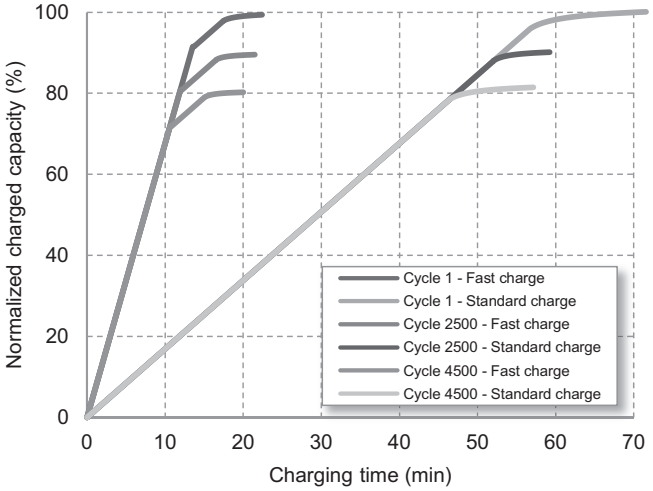

Fig. 8. Normalized charged capacity versus the charging time.

recharged in approximately 20 min, even after 4500 cycles. When compared to the standard charging procedure, the fast charging technique allows the cell to recharge in 1/3rd of the normal time.

The capacity retention as a function of cycle number is shown in Fig. 9. The discharged capacity is normalized to the adopted standard discharged capacity (2.264 Ah at 1 C) measured during conditioning. The initial cycles with the fast charging cycling procedure and 4 C discharges achieved over 99% of the standard discharge capacity. The capacity fade evolution followed a linear trend that remained consistent throughout the testing: approximately 4% of the capacity was lost after every 1000 cycles. The USABC defines the end-of-life of a cell as that point at which a specific test protocol cannot deliver more than 80% of its nominal capacity [5]. The long-term goal defined by the USABC for cycle life is set at 1000 cycles. Our definition of 2.264 Ah as the nominal capacity suggests that the cell will reach its end-of-life after approximately 5000 cycles, while still maintaining a coulombic efficiency near 100%.

3.3. Cycling scheme: temperature, energy and internal resistance results

The evolution of the cell temperature and the current profile through two complete cycles are shown in Fig. 10. There is a 2 min rest between each charge and discharge cycle. The cell temperature increased rapidly during the 4 C discharge cycles. With the first stage at 4 C, the temperature rose again after a slight decrease until it was approximately the value at the end of each discharge cycle. The lower current in the last two stages allowed the cell temperature to decrease abruptly to its lower values near the thermal chamber preset point (23 °C).

Fig. 11 shows a more detailed cell temperature evolution through the entire experiment. The cell temperature never rose above 30 °C; its maximum values averaged 28 °C and the average cell temperature was 27 °C. The minimum temperature values reached at the end of the CV–I charging stage were slightly above the chamber temperature.

Fig. 12 shows the Ragone plot, which reveals the specific energy (Wh kg^{-1}) versus the specific power (W kg^{-1}) delivered by the cell as cycling progresses. This plot shows the trade-off between how much energy is available and how fast it can be delivered. The curves follow a downward linear trend and show a specific energy degradation of approximately 4% for every 1000 cycles; despite this decrease, the cell can still deliver over 75 Wh kg^{-1} at power demands near 400 W kg^{-1}, even after 4500 cycles.

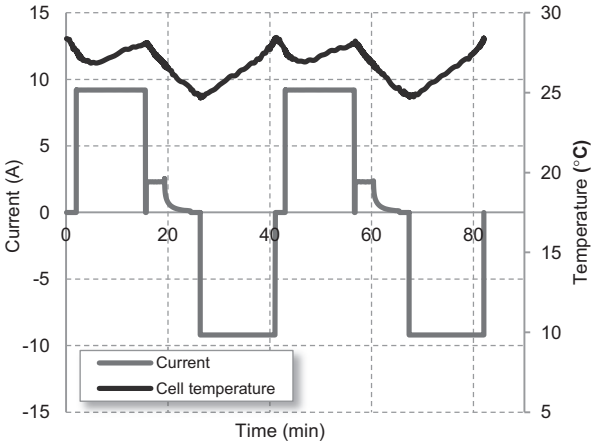

Fig. 10. Cell temperature and current evolution during cycling.

The cell's charged and discharged energies, both in the continuous cycling (continuous fast charging and 4 C discharging) and the reference tests (standard 1 C rate charge/discharge), are compared in Fig. 13. The discharge energy delivered at 4 C is lower (by approximately 8%) than the discharge energy at 1 C measured in the reference tests. However, the energy required to fast charge the cell is very close to the energy needed for a standard charge; the energy difference between the two procedures (fast and standard) remains less than 2.5% throughout the cycling life and indicates that the proposed fast charging procedure is an improvement over the standard procedure.

Energy efficiency is defined by the USABC as the ratio of the net DC energy delivered by a cell during a discharge to the total DC energy required to restore the initial SOC [5]. From the curves depicted in Fig. 13, the calculated energy efficiency is approximately 88% when cycling under fast charging and 4 C discharging and 95% under standard conditions (1 C rate charge/discharge).

The internal resistance of a Li-ion battery is divided into an ohmic and a polarization component [20,21]; the measurements carried out in these tests include the sum of both. The internal resistance measurements were calculated at 50% SOC during both charging and discharging according to Eq. (1), from the voltage difference between the C/25 and 4 C charge and discharge rates. The results shown in Fig. 14 indicate that the internal resistance variation is small during the first 4000 cycles and that a small increase of 7% occurs when approaching the end of the cycle life. The

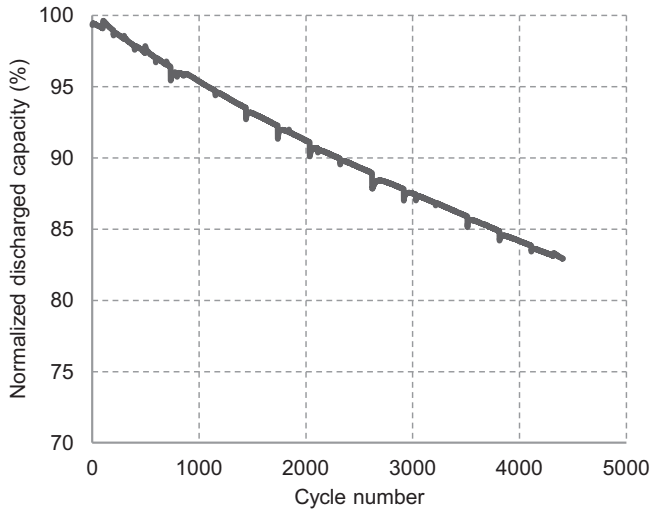

Fig. 9. Discharged capacity evolution with cycling.

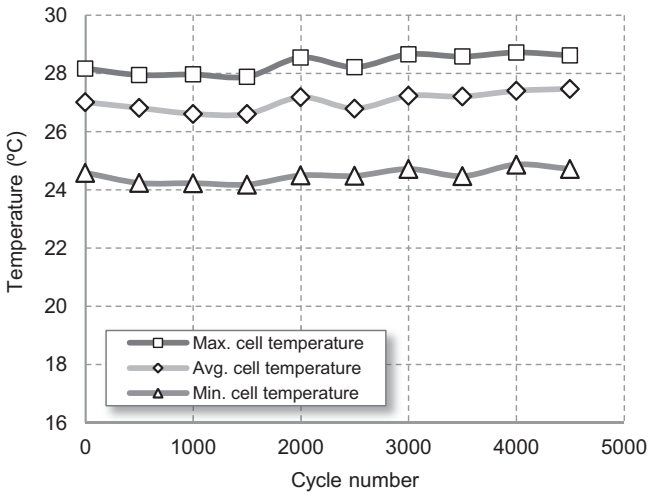

Fig. 11. Cell temperature evolution during cycling.

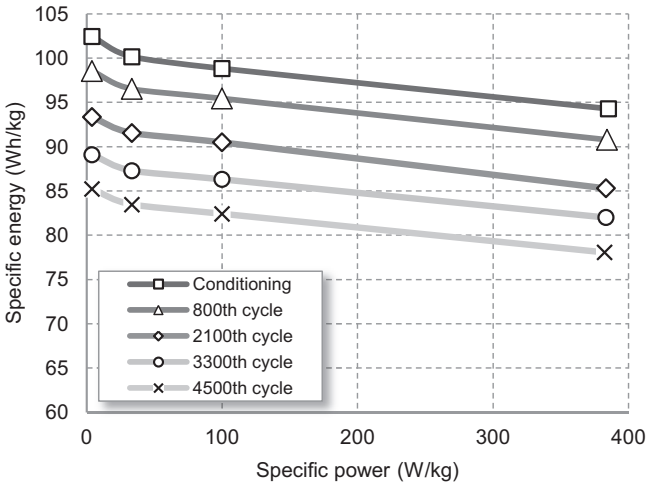

Fig. 12. Evolution with cycling of the Ragone plot.

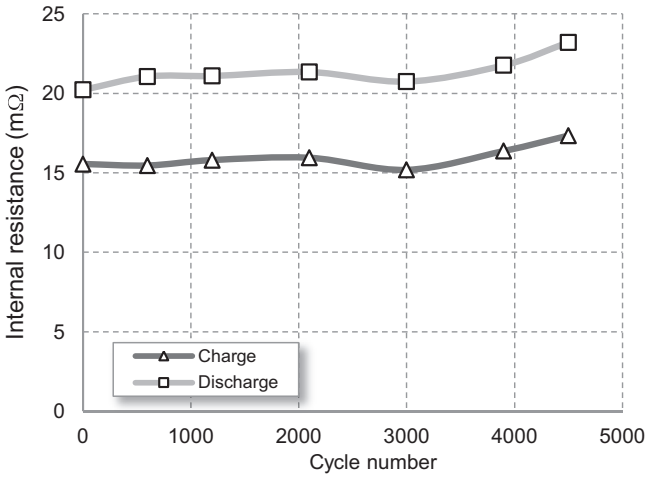

Fig. 14. Internal resistance evolution with cycling, both in charge and discharge cycles.

internal resistance values were found to be lower for charging currents than for discharging currents, in agreement with the discussion in Ref. [19].

4. Discussion

A multistage fast-charging technique was proposed and tested on a high power LFP cell. The USABC long term goal for fast charging was demonstrated; the cell can be fully charged within 20 min, thus reducing the charging time by 65% when compared with the manufacturer's recommended standard charge at 1 C. In addition, the proposed fast charging adds little energy loss, as it only uses 2.5% more energy compared to the standard charging procedure.

These results were achieved by splitting the charging process into three different stages. The highest charging current (4 C) is applied when the cell's internal resistance is in its lower and plateau values. This strategy reduces the energy losses that result from heating due to internal resistance. Almost 90% of the cell's capacity is charged during the first stage (CC-I), although the stage uses only 60% of the total charging time. Then, when the internal resistance value increases and the cell begins to heat up, the charging current decreases in two final stages (CC-II and CV-I) that consume the remaining 40% of the total charging time. The final stages charge only 10% of the cell's capacity and allow the cell's temperature to decrease rapidly, thus decreasing the cell's risk of overheating. The charging process avoids the condition of high cell potentials over long periods because the constant voltage charge stage is set to last for only 5 min. These combined features of the multistage fast charging protocol help the cell to reduce its main aging mechanism.

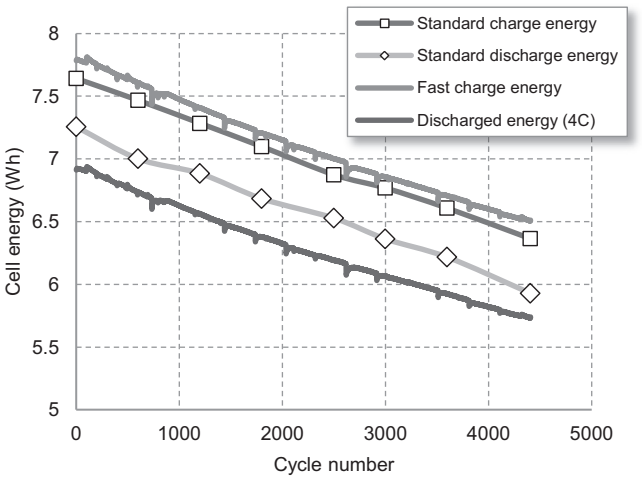

Fig. 13. Cell energy in charge and discharge through cycling.

The main degradation factors in Li-ion cells consist either of a loss of lithium inventory, a loss of active material, a rise in the cell impedance, and/or a physical degradation of the cell [6,11,22,23]. These degradation effects are accentuated at high cell temperatures; however, because the tested cell never reached temperatures above 30 °C under the proposed testing scheme, high temperatures did not accelerate its aging mechanisms.

The USABC life cycle target goal of 1000 cycles was demonstrated: 4500 cycles were completed and resulted in 83% of the cell's initial capacity remaining. If it is assumed that one complete cycle is performed per day, the equivalent of over 13 years of service life would have been achieved by the cell under the proposed cycling conditions. The capacity evolution demonstrated a linear trend versus the cycling number and remained linear during the whole experiment; this characteristic is valuable in predicting the battery's end of life in BMSs or other control systems.

The 4 C discharge rate carried out on the cell reached a power capability of 400 W kg^{-1}, which is the long-term USABC goal regarding specific power. The Ragone plot demonstrates that the power capability of the cell remains inalterable, even after 4500 cycles. This result is directly linked to the internal resistance, which remained almost constant through the cycles. This lack of decrease in the power capability of the cell is a crucial feature for EVs and PHEVs, which are required to have a fast acceleration response and good performance under high-demand load currents. These results indicate that the cell loses performance with cycling due to a loss of capacity, instead of a rise in the internal resistance. This behavior has also been observed in a study carried out on the same LFP cells [23]. Another experiment carried out on the same cell also revealed that capacity fade was very small and internal resistance did not increase significantly after 2000 cycles [24]. This result confirms that the proposed multistage fast charging technique does not introduce any relevant factors that accelerate the deterioration of the cell.

The values of the specific energy (Wh kg^{-1}) are below average when compared to other Li-ion technologies such as LCO or NCA [8,25]; despite this lack of performance, the cells met the mid-term

objectives from the USABC (80 Wh kg^{-1}). The efficiency of the charge/discharge process is quite high and meets the long-term USABC goals, demonstrating values above 94% for C rates and up to 99% for C/25 rates. However, along with low specific energies, the main drawback for the tested cell is its price: even if an inexpensive cell ($15/unit) is assumed, the final price of an entire system with hundreds of cells to power an EV would easily be much higher than the final USABC goal of $100/kWh.

5. Conclusion

A multistage fast charging technique for a high power LFP cell was proposed in this work. The technique met the USABC goals regarding fast charging; the results show that a fully discharged cell can be recharged within 6 min—40% of its rated capacity, it can be fully recharged within 20 min, and the energy required for the fast charging process is nearly the same as that required for a standard charge.

An extended cycle life test was also carried out to study degradation effects. The results reveal that, even after a total of 4500 cycles only capacity fade was observed. A Ragone plot and measurements on the internal resistance show that the fast charging protocol and testing scheme barely affected the cell power capability. Moreover, the fast-charging technique did not overheat the cell because the charging was divided into three different stages. As a result, the cell was better maintained.

The cell's overall performance can be considered to be satisfactory. In particular, we emphasize the cycle life and power capability: the cycle life is predicted to be over 5000 cycles while maintaining a, essentially invariable power capability. Despite these advantages, the battery's weight and final cost are two characteristics that must be improved to achieve the widespread application of this type of cell for use in EVs.

Experiments are actually being carried out, in order to identify the cell performance and aging mechanisms under test conditions of higher and lower ambient temperatures. Similarly, realistic road tests could be performed to evaluate the cell's behavior under EV driving conditions.

Acknowledgments

The authors would like to thank the Spanish Ministry of Science and Innovation (MICINN) who provided the funding (TEC2009-12552) for this work.

References

[1] Z.E. Renault, http://www.renault-ze.com/en-gb (accessed 10.06.12).
[2] Mitsubishi i-MiEV, http://www.mitsubishi-cars.co.uk/imiev/ (accessed 10.06.12).
[3] SAE Electric Vehicle and Plug-in Hybrid Electric Vehicle Conductive Charge Coupler, SAE JI.
[4] M. Yilmaz, P.T. Krein, in: Electric Vehicle Conference (IEVC), 2012 IEEE International, 2012, pp. 1—8.
[5] United States Advanced Battery Consortium. Electric Vehicle Battery Test Procedures Manual, USABC, January 1996. http://www.uscar.org/guest/publications.php (accessed 10.04.12).
[6] J. Vetter, P. Novák, M.R. Wagner, C. Veit, K.C. Möller, J.O. Besenhard, M. Winter, M. Wohlfahrt-Mehrens, C. Vogler, A. Hammouche, J. Power Sources 147 (2005) 269.
[7] C. Pillot, European Electric Vehicle Congress (EEVC), Brussels, 2011.
[8] A. Burke, M. Miller, J. Power Sources 196 (2011) 514.
[9] B. Scrosati, J. Garche, J. Power Sources 195 (2010) 2419.
[10] D. Jugović, D. Uskoković, J. Power Sources 190 (2009) 538.
[11] W.J. Zhang, J. Power Sources 196 (2011) 2962.
[12] S. Chung, J.T. Bloking, Y. Chiang, Nat. Mater. 1 (2002) 123.
[13] P.H.L. Notten, J.H.G. Veld, J.R.G. Beek, J. Power Sources 145 (2005) 89.
[14] A. Burke, M. Miller, H. Zhao, Electric Vehicle Symposium (EVS 26), Los Angeles, 2012.
[15] S.S. Zhang, J. Power Sources 161 (2006) 1385.
[16] M. Dubarry, B.Y. Liaw, J. Power Sources 194 (2009) 541.
[17] A123 Systems, Inc, http://www.a123systems.com/products-cells-26650-cylindrical-cell.htm (accessed 10.06.12).
[18] I. Bloom, S.A. Jones, E.G. Polzin, V.S. Battaglia, G.L. Henriksen, C.G. Motloch, R.B. Wright, R.G. Jungst, H.L. Case, D.H. Doughty, Journal of Power Sources 111 (2002) 152.
[19] M.A. Roscher, J. Vetter, D.U. Sauer, J. Power Sources 191 (2009) 582.
[20] B.Y. Liaw, G. Nagasubramanian, R.G. Jungst, D.H. Doughty, Solid State Ionics 175 (2004) 835—839.
[21] M. Dubarry, N. Vuillaume, B.Y. Liaw, J. Power Sources 186 (2009) 500—507.
[22] M. Dubarry, B.Y. Liaw, M.S. Chen, S.S. Chyan, K.C. Han, W.T. Sie, S.H. We, J. Power Sources 196 (2011) 3420.
[23] P. Liu, J. Wang, J. Hicks-Garner, E. Sherman, S. Soukiazian, M. Verbrugge, H. Tataria, J. Musser, P. Finamoer, J. Electrochem. Soc. 157 (2010) A499.
[24] S.B. Peterson, J. Apt, J.F. Whitacre, J. Power Sources 195 (2010) 2385.
[25] T.B. Reddy, D. Linden, Linden's Handbook of Batteries, fourth ed., McGraw Hill, New York, 2011.